

Glancing ion incidence on Si(100): Influence of surface reconstruction on ion subsurface channelingYudi Rosandi^{1,2} and Herbert M. Urbassek^{1,*}¹*Fachbereich Physik und Forschungszentrum OPTIMAS, Universität Kaiserslautern, Erwin-Schrödinger-Straße, D- 67663 Kaiserslautern, Germany*²*Department of Physics, Universitas Padjadjaran, Jatinangor, Sumedang 45363, Indonesia*

(Received 7 November 2011; revised manuscript received 29 February 2012; published 13 April 2012)

We demonstrate that a Si target may exhibit the phenomenon of subsurface channeling for glancing incidence ions. To this end, we perform molecular-dynamics simulations of 3 keV Ar⁺ ion impact at grazing incidence (83° toward the surface normal) on a Si (100) surface. Both an unreconstructed and a (2 × 1) dimer-reconstructed surface are investigated. In both cases, the ion is reflected from the flat terrace and creates neither damage nor sputtering. The situation changes when a surface step is introduced on the surface; ion incidence in the vicinity of the step induces both damage and sputtering. We find that the phenomenon of subsurface channeling plays a dominant role in damage creation at the step edge. Subsurface channels aligned in the ⟨110⟩ direction are created under the reconstructed surface; they run parallel to the dimer rows. If the ion incidence geometry is favorable—incidence azimuth aligned along ⟨110⟩ and the ion approaching an unbonded B step—the ion can enter these channels. Without surface reconstruction no subsurface channeling can occur. Subsurface-channeled ions generate peculiar surface damage patterns which may allow their identification in experiment.

DOI: [10.1103/PhysRevB.85.155430](https://doi.org/10.1103/PhysRevB.85.155430)

PACS number(s): 79.20.Rf, 61.80.Jh, 79.20.Ap

I. INTRODUCTION

Surface patterning of silicon by ion bombardment has been studied in the recent past.^{1–3} Particular attention has been paid to the ripple patterns induced by ion impact at normal and off-normal incidence angles.⁴ However, the effect of single-ion impacts at glancing incidence on the flat silicon surface has, up to now, not been sufficiently evaluated.

It is known that, at glancing incidence, ion impact creates distinctive damage on the bombarded surface. The underlying mechanisms have been studied in detail for a metal surface, Pt (111).^{5–8} Under this condition, pre-existent surface defects play an essential role in transferring the ion energy to the target crystallite. In particular, the existence of surface steps enables a very special type of ion trajectory, which features the so-called subsurface-channeling phenomenon. Its characteristic is the creation of an aligned row of periodic damage islands. Using a suitably massive ion, it is also possible to generate a vacancy groove decorated with adatom islands on its sides.^{9,10}

In this paper, we study glancing-ion incidence on the Si (100) surface at incidence angles where the flat terrace reflects the ion, and only surface steps allow them to perform sufficiently violent collisions to induce damage at the surface and sputtering. We focus on the possibility that the ion enters the target in a subsurface-channeled trajectory and elucidate the role of this phenomenon for target modification and sputtering.

Our prediction of subsurface channeling in a Si crystal was not anticipated. Compared with the well-studied case of Pt, Si crystals differ strongly in their crystal structure and in their possibility of surface reconstruction. In addition, Si atoms are lighter than typical projectile ions (Ar in our case), while Pt is much heavier; thus the response of the target (damage—in particular destruction of the channels while the projectile passes through it) is expected to be larger than in Pt. We believe that our results will also be interesting in the field of surface patterning and ripple formation of Si surfaces under glancing-ion impact, since we describe the damage processes

occurring under individual-ion impact. The generation of surface damage aligned in the ion-incidence direction, such as we describe it here, may influence the damage patterns evolving under higher fluences.⁵ While continuum theories of surface topography evolution are quite developed,^{11,12} their need for atomistic input has recently been acknowledged.^{13,14} Our work demonstrates the anisotropic damage developing under grazing-incidence ion impact on Si, such as is relevant for ion-induced surface topography modification.

The Si (100) surface usually exhibits the (2 × 1) reconstruction during which dimer rows, aligned in [110] direction, are created.¹⁵ These dimer rows form subsurface channels, which are able to trap the incoming ions. We shall show that, when an incoming ion impinges at glancing incidence in front of a monolayer surface step, it can enter the channel and propagate in it for a relatively long distance below the dimer rows. During channeling the reconstruction pattern is destroyed and surface defects, vacancy islands, and other extended defect structures are left behind. The defects are aligned in the ion-propagation direction. An unreconstructed surface does not exhibit surface channeling, since the channels formed by the dimer rows do not exist. As a consequence the damage patterns on this surface differ considerably from those on the reconstructed surface. For the unreconstructed surface, channeling is only possible in deeper layers or inside the bulk, when ions penetrate the surface layers. Besides the surface damage produced by glancing-ion impact, we shall also discuss the consequences on sputtering. We shall demonstrate that a monolayer step leads to strong sputtering; again the features found for reconstructed and unreconstructed surfaces differ in a characteristic way.

II. SIMULATION METHOD

We consider a Si (100) target consisting of 100 926 atoms; it extends 310 Å in the direction of the ion beam, has a width of 160 Å, and is 40 Å thick. A monolayer step is created on the surface by removing the topmost atomic layer up to the position $x = 103$ Å; the remaining

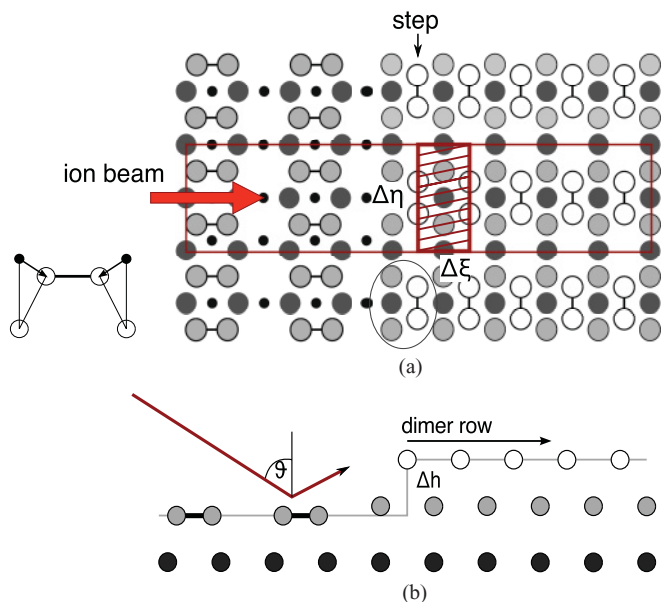


FIG. 1. (Color online) Ball model of the target crystal, (a) top view, (b) side view. The dimers are shown by two circles connected by a line. White circles denote upper-layer atoms, gray circles denote second-layer atoms, and black circles denote third-layer atoms. The atoms in the fourth layer are drawn as small black dots, and only under the lower terrace. The step position is indicated by a black arrow. The dimer reconstruction of the surface is shown as a side view in the inset in (a), where the arrows denote the shift of the black atoms during reconstruction. The large rectangle denotes the impact area of the ion used in the simulation. The smaller rectangle (shaded) shows a unit impact cell for the coordinates $\xi = 0$ and $\eta = 0$. The size of the unit cell is $\Delta\xi \times \Delta\eta = 3.84 \times 7.68 \text{ \AA}^2$. The ion beam is aligned with the $[110]$ azimuth, as indicated by the red arrow. Ions impinge with an angle ϑ of incidence with respect to the surface normal. Δh denotes the height of the monatomic surface step.

207 \AA then form the upper terrace (see Fig. 1). The upper terrace will allow the propagation of subsurface-channeled ions under it. We consider both a target with an unreconstructed (100) surface, and a target with a (2×1) dimer-reconstructed surface. The dimer rows on the upper and on the lower terrace are oriented in the $\langle 110 \rangle$ direction, but are orthogonal to each other. The step is parallel to the dimers of the upper terrace (see the sketch in Fig. 1) and is called an *unbonded B step*.¹⁶

We model the interaction between Si atoms using the Stillinger-Weber potential.¹⁷ The potential is splined to the repulsive Ziegler-Biersack-Littmark (ZBL) potential¹⁸ toward high energies. This potential predicts an (untilted) dimer reconstruction of the surface. After relaxation, we observe that the dimer atoms moved 0.76 \AA toward each other and 0.1 \AA toward the surface [see inset of Fig. 1(a)]. These shifts are in reasonable agreement with experimental and theoretical data.^{19–21}

Ar^+ ions with an energy of $E = 3 \text{ keV}$ and impact angle $\vartheta = 83^\circ$ with respect to the surface normal impact the surface in the vicinity of the surface step. The interaction between the impinging ions and the Si atoms is modeled by the repulsive ZBL potential, which is cut off at 3.2 \AA . The ion-incidence azimuth is aligned with the $[110]$ direction, such that the ions

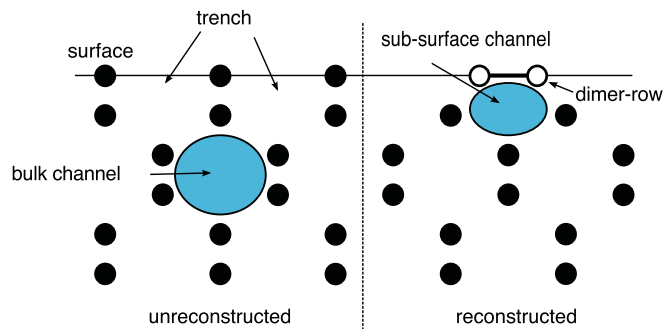


FIG. 2. (Color online) Sketch of $\langle 110 \rangle$ cross section of Si (100) surface, showing unreconstructed (left) and reconstructed (right) surface. The channels are marked by blue ellipses; here only two exemplary channels are shown. The dimer row is indicated by white balls.

fly parallel to the dimers on the lower terrace, but perpendicular to the dimers of the upper terrace (see Fig. 1).

The target crystal is relaxed to minimum potential energy by quenching its kinetic energy; thus it has zero temperature at the start of the simulation. While the top surface is free, the outermost layers of the other five boundaries are kept fixed. In addition, these boundaries contain a 7.68- \AA -wide layer of damped atoms; according to the recipe by Beeler²² the damping constant has been chosen to mimic a critically damped oscillator at the Debye frequency of Si. We checked that our damping boundary conditions absorb any (elastic) pressure wave emitted from the projectile with high efficiency. We note that we also verified that our simulation cell size is sufficiently large by performing test simulations with varying cell sizes and choosing the size above which results (in damage and sputtering) did not change.

We simulate ion-impact points within a stripe of width 7.68 \AA , which due to symmetry is representative of the entire surface. The length of the stripe (perpendicular to the step) is chosen such that the ion-impact zone covers completely the influence zone of the step. We choose coordinates on the surface (at the height of the upper terrace) to identify the ion-impact points: ξ denotes the coordinate parallel to the ion-incidence azimuth, and η is the lateral direction.

An elementary surface cell of the dimer-reconstructed surface is shown in Fig. 1; it has dimensions $\Delta\xi \times \Delta\eta = 3.84 \times 7.68 \text{ \AA}^2$. We simulate 50 impacts inside each such elementary surface cell; the impact points are selected randomly within the cell. In total 1000 impact events are simulated in 20 cells. We checked that ion impact outside the impact zone leads to vanishing sputtering and damage formation. For the unreconstructed surface, we simulate only 20 impact points per elementary surface cell.

III. THE $\langle 110 \rangle$ CHANNELS

Figure 2 shows a sketch of the subsurface and bulk channels in $\langle 110 \rangle$ directions. In the unreconstructed surface, one encounters no subsurface channel directly below the first layer terrace; in this case, the surface forms “V”-shaped trenches parallel to the ion direction. These trenches will lead to reflection of the incoming ions. However, surface reconstruction closes the “V”s and a new *subsurface channel*

in the $\langle 110 \rangle$ direction is created. These subsurface channels are smaller than the bulk channels.

Ions cannot directly enter a channel under a flat terrace. However, the existence of a surface step enables impinging ions to enter a channel and then to propagate in it.

In previous work,^{7,8,23,24} we determined that ions interact with the step—and can enter a subsurface channel—only if their impact point is within a region $-x_c < \xi < 0$; that is, not farther than the *critical distance* x_c away from the step edge. For a flat terrace, x_c is given by a simple geometrical criterion,²⁵

$$x_c^{\text{flat}} = 2\Delta h \tan \vartheta. \quad (1)$$

Here, Δh is the step height, which amounts for a monolayer step to $\Delta h = a/4 = 1.36 \text{ \AA}$, where $a = 5.43 \text{ \AA}$ is the lattice constant of Si. However, we found that, for atomically rough surfaces, the simple geometrical value x_c^{flat} underestimates the zone of influence of the step edge.⁹ We obtain a better estimate by noting that the step height is $2\Delta h$ when seen from the bottom of the V-shaped troughs (cf. Fig. 1), and thus

$$x_c = 4\Delta h \tan \vartheta, \quad (2)$$

which gives $x_c = 44 \text{ \AA}$. This value applies for ions incident along the bottom of the trough and approaching the dimers situated on the upper terrace.

Figure 3 shows the potential inside the channels in the continuum approximation. The contours represent equipotential lines between atomic strings inside the crystal. These strings lie inside the green circles in the high-potential-energy areas. The impinging ion interacts with the strings of Si atoms by the repulsive ZBL potential. In the continuum approximation, the scattering from an individual atom in a string is substituted by a continuous potential field.²⁶ In Fig. 3, we measure the potential energies with respect to the potential in the center of a channel. We note that this continuum picture of the channel is included here to provide a semiquantitative description of the potential energy in the channel, and of possible pathways for channel switching and dechanneling. Since Ar is a massive projectile (relative to a Si atom), the channel will be dynamically distorted during the passage of the ion; such distortions are not included in the continuum description.

Figure 3(a) shows the potential of an (unreconstructed) channel under an unreconstructed surface. This channel lies in the second layer of the crystal; it is identical to a channel in bulk Si. This channel is not directly accessible to an impinging ion; entrance would only become possible by switching from another channel. In contrast, we see first-layer subsurface channels in the reconstructed surface shown in Fig. 3(b). In this case the channel is narrower than the previous one. This discussion already indicates that second-layer channeling will only be possible in surface-reconstructed Si.

The motion of a channeled ion is constrained to the region inside a certain equipotential line, corresponding to its *perpendicular* kinetic energy component,

$$E_{\perp} = E \cos^2 \vartheta. \quad (3)$$

Ions that are trapped inside a channel move almost parallel to the channel axis and thus perpendicular to the plane of

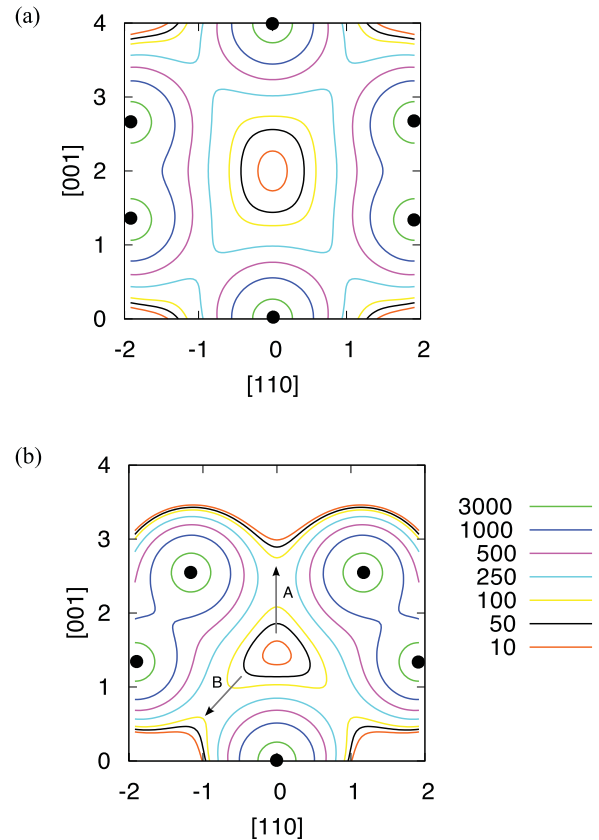


FIG. 3. (Color online) Equipotential lines (energies measured in eV) of the continuum potential inside $\langle 110 \rangle$ channels. The atomic strings are marked by black dots inside the green circles. (a) Bulk channel, (b) reconstructed subsurface channel. The arrows shown in (b) denote paths along which a channeled ion may escape from the channel (A) or switch to a deeper channel (B). Lengths are indicated in \AA .

the potential plot in Fig. 3. Thus, their perpendicular kinetic energy (E_{\perp}) is small and the ion is constrained inside a small area bounded by the equipotential line E_{\perp} . The perpendicular energy of a 3 keV ion impinging at an 83° angle of incidence amounts to $E_{\perp} = 45 \text{ eV}$, so the ion is channeled roughly inside the area bounded by the black line (50 eV contour).

The arrows in Fig. 3(b) show the paths that an ion may take in order to escape from the channel or to switch into a deeper-layer channel. Each path passes through a saddle point between two adjacent atoms. For escape or channel-switching, the ion has to overcome the potential barrier of the saddle point. In our case, escape (path A) requires 147 eV and channel switching (path B) requires 270 eV.

The continuum approximation assumes that the target atoms are fixed and do not move during the channeling motion. However, since Si atoms have a smaller mass than the projectile ion, the potential walls shown by the contours are relatively soft, since in reality Si atoms will move. In this case, the motion of a channeled ion is not so rigidly confined inside the equipotential lines. The barriers can be more easily overcome and the escaping and channel-switching events may occur more frequently.

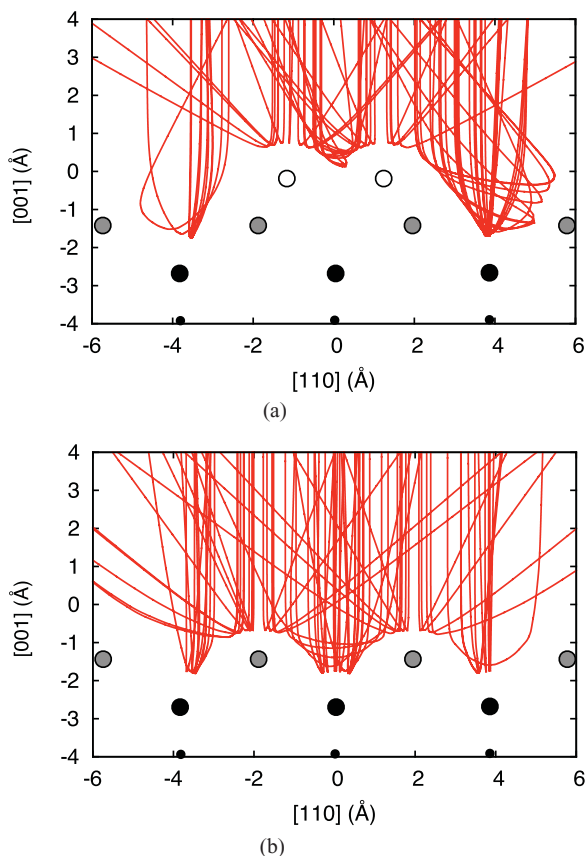


FIG. 4. (Color online) Trajectories of ions impinging on the upper terrace (a) and on the lower terrace (b) of the dimer-reconstructed surface. Dots denote target-atom positions. The trajectories are projected onto the plotting plane perpendicular to the (110) direction.

IV. ION TRAJECTORIES AND SUBSURFACE CHANNELING

In this section, we study trajectories of ions incident on the reconstructed Si surface. Figure 4 shows the projection of ion trajectories onto the plane perpendicular to the ion-beam direction. The ions impinge on the lower and upper terrace of the target, far from the step. In this case we find that neither ion penetration below the surface nor sputtering occurs in our simulations. This demonstrates that violent collisions leading to surface damage or sputtering may only occur in the vicinity of the surface step. The plot gives information about the high lateral corrugation of the Si (100) surface, which amounts to around 2.5 \AA ; we measure this as the difference between the approach distance of ions impinging into a dip of the V and the peak region above the dimer atoms. The approach distance of ions to the atomic string is around 0.8 \AA . The surface corrugation of the lower terrace is less than that of the upper terrace since one atom layer is missing on the lower terrace. The lower-terrace corrugation amounts to 1.2 \AA .

Ions impinging close to a step behave quite differently. Figure 5 shows several exemplary trajectories impinging at around $x_c/2$ in front of the step. The cross-sectional view in Fig. 5(a) can be directly compared with that for a terrace [Fig. 4(a)]. Again, ion impact into the V-shaped grooves leads to reflection; the projectile cannot enter a channel. However, if the ion is approaching in a trench that is terminated

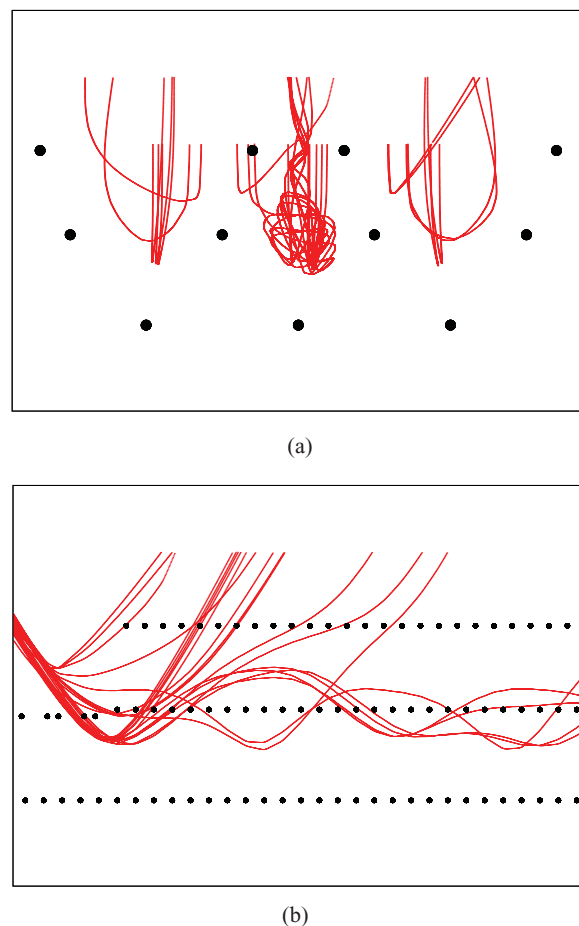


FIG. 5. (Color online) 20 exemplary ion trajectories (impact at $\xi = 23 \text{ \AA}$): (a) cross-sectional view along the incidence azimuth, (b) side view. The plot shows three cases: specular reflection of ions impinging on the V regions of the lower terrace; short channeling events, where ions dechannel after the first reflection from the bottom of the channel; and long-channeled trajectories. Black dots denote the positions of target Si atoms.

by the dimer on the upper terrace, a completely different picture results: the projectile is captured in the reconstructed subsurface channel. We thus see that surface reconstruction divides the impact area into an effective and an ineffective region. Ions hitting the ineffective region do not contribute to damage formation or sputtering.

In Fig. 5(b), we observe these trajectories from the side. Three types of trajectories can be discerned: (1) specularly reflected trajectories, (2) short-, and (3) long-channeled trajectories. Type (1) encompasses all those ions that impinge on the V-shaped grooves that are not terminated by an upper-terrace dimer. In this situation the ions are not able to produce violent collisions, and the impact is completely unproductive. The channeled trajectories of type (2) immediately dechannel after their first reflection from the bottom of the channel wall. The immediate dechanneling demonstrates the low escape barrier that an ion has to overcome [cf. path A in Fig. 3(b)]. Trajectories of type (3) perform several oscillations in the channel, creating relatively long trajectories. Note that their form is far from sinusoidal; this is due to the strong deviation of the channel from a cylindrical shape.

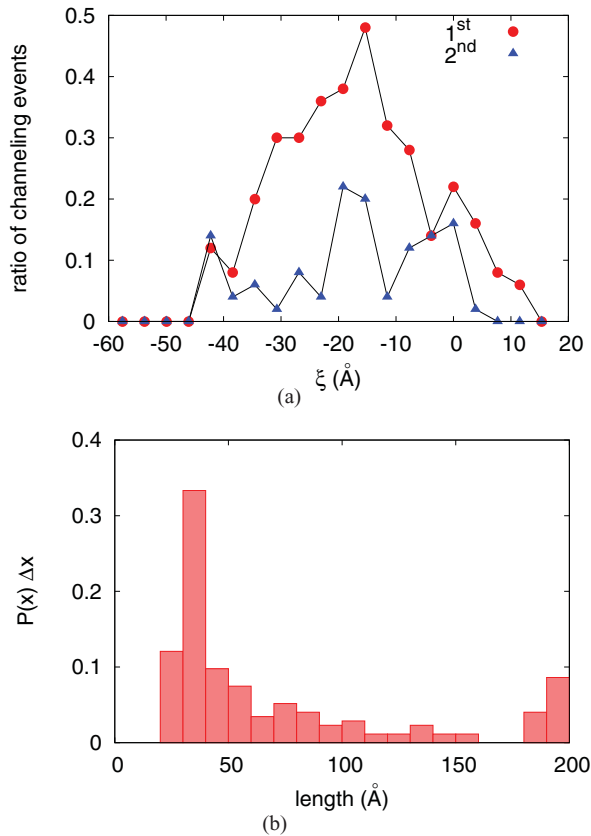


FIG. 6. (Color online) (a) Probability of channeling as a function of the ion-impact coordinate ξ . Red dots, first-layer channeling; blue triangles, second-layer channeling. The step is positioned at $\xi = 0$. (b) Distribution $P(x)\Delta x$ of the channeling length x , Δx is the histogram width of 10 Å.

We now discuss in quantitative detail the probabilities for subsurface channeling and the lengths of channeled trajectories. In agreement with the nature of the axial $\langle 110 \rangle$ channel, we define our channeling criterion as follows: Consider the three channels that are accessible to the ions; viz. the reconstructed subsurface channel facing the impact zone and the two second-layer channels to the left and right of it [cf. Fig. 2(b)]. Ions propagating outside these channels may be grouped as reflected, implanted, or dechanneled; they will not be considered further here. We measure the propagation length of an ion inside a cylinder of radius $R = 1.5$ Å centered in the channel. The length is measured with respect to the step position. We consider only those particles as channeled which traveled at least a distance $x_c/2 = 22$ Å, thus making sure that the projectile performed at least half an oscillation period inside the channel. This criterion is in agreement with that used by us in earlier work for subsurface channeling under the Pt (111) surface.²⁴ The maximum channeling length which we can detect amounts to 200 Å, in accordance with the size of our simulation crystallite.

We collect the results of our channeling analysis in Fig. 6. We observe channeling events in an impact zone extending from $\xi = -45$ Å in front of the step to $\xi = +15$ Å behind the step. The extent of the zone in front of the step is in good agreement with the geometrical distance x_c [Eq. (2)]. Even impacts on the upper terrace may lead to channeling, since

the dimers near the step have a weaker bonding compared to those situated in the middle of a clean terrace, and they are more flexible, allowing an ion to penetrate the surface. The channeling probability peaks at almost 0.5 close to the middle of the impact zone. This is an astonishingly high value since it means that all ions impinging in the V-shaped groove leading to the dimer on the upper terrace will enter the reconstructed subsurface channel; those that impinge in the grooves, which do not lead to the dimer, are reflected from the surface anyway. Not unexpectedly, the fraction of ions channeled in the second layer is considerable and amounts to 37% on average. These are ions that were initially channeled in the reconstructed subsurface channel, but then escaped to a deeper-lying channel via path B [cf. Fig. 3(b)]. Note the peculiar situation at $\xi = -42$ Å, where more ions channel in the second layer than in the first layer. At this impact point, ions hit the step atoms from below, after reflection off the lower terrace. Thus the ion trajectory may become deflected downward, into the target inner. In some cases the ions fly along path B and become captured in the second-layer channel.

Figure 6(b) shows the distribution of the channeling lengths. The highest probability is attributed to trajectories with a short length of around 35 Å. This fact indicates that most of the channeled ions escape after their first reflection from the bottom of the channel. This gives further evidence to the fact that the energy barrier to dechanneling is quite small. Beyond this maximum, the distribution quickly decays, such that high channeling lengths >100 Å occur only rarely. We conclude that the typical fate of a channeled ion is to travel only a small path in the channel (of the order of x_c) and then to dechannel.

The discussion in this section has been restricted to ion impact on the reconstructed Si surface, since we focused on clarifying the conditions under which subsurface channeling occurs. For the unreconstructed Si surface, we found that the probability that ions enter a channel is negligible.

V. SURFACE DAMAGE

We classify the damage induced by ion impacts into three classes: (1) damage due to direct ion impact onto the step atoms, (2) daughter island creation due to dechanneling of the ion at some distance behind the step, and (3) destruction of dimer rows by long-channeling events.

Figure 7 presents snapshots of exemplary events corresponding to this damage classification. The damage class (1) shown in Fig. 7(a) is typical of a direct-hit event. The ion may transfer a large amount of energy to an edge atom while it penetrates the surface and is implanted below the step. Such a violent collision leaves a relatively large crater close to the step. This type of damage erodes the step and is responsible for the retraction of the step edge under continued beam exposure.

The second class of damage (daughter-island creation) is represented by Fig. 7(b). This kind of event is rare. We found only 8 daughter islands in 1000 simulations. This type of damage is created by violent dechanneling events, in which the ion leaves the subsurface channel and exits from the crystal.

The third class of damage is created by a long-channeled ion. This damage is characterized by a relatively elongated destruction of the dimer row below which the ion is channeled.

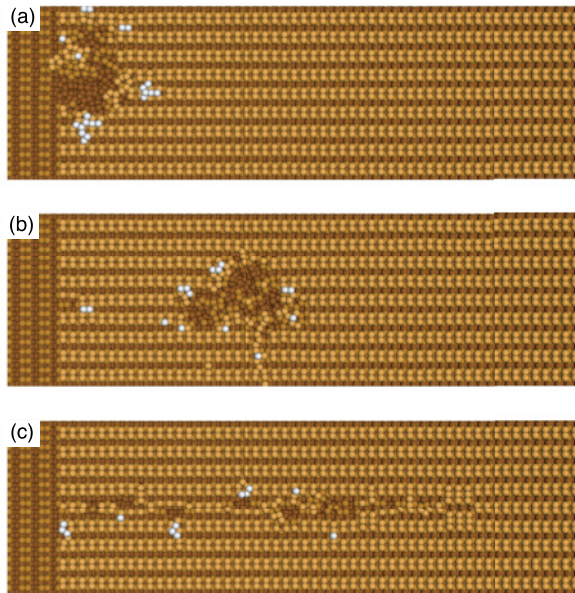


FIG. 7. (Color online) Snapshots of typical surface damage created by ion impact. (a) A violent direct hit onto the step-edge atoms; (b) daughter island formation; (c) damage resulting from a channeled ion. Color codes the height of the atoms from dark (downmost) to light (top layer on upper terrace).

The ion breaks the dimers and propels the atoms to the side of the dimer row. In contrast to our findings for the Pt (111) surface,⁷ in Si (100) we cannot find a fixed oscillation period (wavelength) of the channeled ion. This is due to the triangular profile of the potential in the reconstructed subsurface channel (cf. Fig. 3); thus, the wavelength depends on the entry point of the ion into the channel.

Figure 8 shows another exemplary long-channeling event. The side view of the ion trajectory shows a nonsinusoidal oscillation. The noncircular nature of the channel may vary the oscillation behavior. Note how the oscillation is reflected by the surface damage. The positions of surface damage not only coincide with the positions where the ion pushes against the upper terrace, but also coincide with where the ion collides with atoms at the sides or bottom of the channel. We surmise that this behavior is due to the angular dependence of the

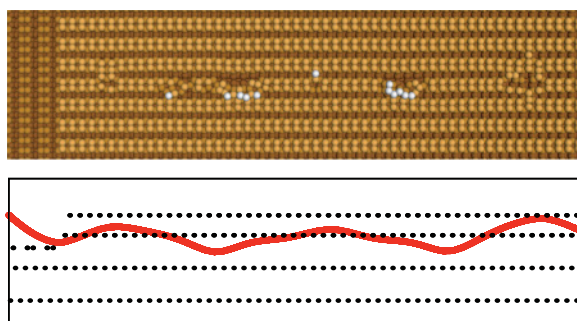


FIG. 8. (Color online) Surface damage created by a well-channeled ion. Upper figure shows a top-view ball model of the target 5 ps after ion impact. Color codes the height of the atoms as in Fig. 7. Bottom figure shows a side view of the ion trajectory (red) for this event. Black dots indicate Si atom positions.

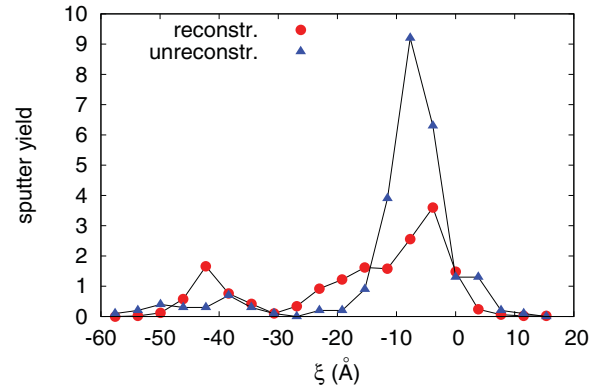


FIG. 9. (Color online) Sputter yield of a 3 keV Ar^+ ion impinging at glancing incidence on a reconstructed (red circles) and an unreconstructed (blue triangles) Si surface. The step is positioned at $\xi = 0$.

binding of Si atoms (many-body interaction). The collision of the ion with atoms below the surface may break some bonds that also affect the bonds of atoms on the surface.

VI. SPUTTER YIELDS

The sputter yield Y is defined as the average number of atoms emitted from the surface due to a single ion impact. In atomistic simulations, we can calculate the sputter yield as a function of the distance ξ from the step position; more precisely, $Y(\xi)$ is the sputter yield averaged over a distance $\xi \pm \Delta\xi/2$, where $\Delta\xi = 3.84 \text{ \AA}$ is the width of the impact unit cell, (cf. Sec. II and Fig. 1). For every ion impact, we monitor the sputter yield Y as the number of all atoms which have left the target in the sense that their potential energy with target atoms is zero.²⁷ Figure 9 shows the simulation results. Here the yields of the reconstructed and of the unreconstructed surface are compared. We first discuss the integral over these quantities,

$$Y^{\text{step}} = \frac{1}{x_c} \int Y(\xi) d\xi, \quad (4)$$

which is called the *step sputter yield* and may serve as an average to quantify our data. From our data we have $Y^{\text{step}} = 1.5$ (2.3) for the reconstructed (unreconstructed) surface. The yield for the unreconstructed surface is higher, since here channeling is suppressed, and hence the possibility of violent collisions, inducing surface damage and sputtering, is larger. Indeed, on the reconstructed surface, where the ion is able to propagate inside the reconstructed subsurface channel, the sputter yield drops by more than 50%. Note that we found that the cases of violent dechanneling, which might lead to productive damage and sputtering [cf. Fig. 7(b)] are rare. More often the ion escapes without much energy loss from a channel into the vacuum and induces only little sputtering.

In order to assess the size of the sputtering yield, we compare to the sputter yield at normal incidence, which has been repeatedly measured: for 3 keV Ar impact at normal incidence it amounts to around 1.2.^{28–30} This comparison demonstrates that the step sputter yield is surprisingly large; remember that at 83° incidence, a flat terrace leads to zero sputtering. The peak sputter values for glancing impact surpass

this value strongly, in particular for the unreconstructed surface. This occurs when the ion impinges directly on the step edge leading to maximum damage and sputtering.

The spatial profile of the sputter yield distribution in Fig. 9 shows two peaks. This behavior has also been found in the sputtering of Pt at grazing incidence.^{8,24} The peak closer to the step edge ($\xi \cong -10 \text{ \AA}$) is connected to direct-hit events, in which the ion directly collides with step-edge atoms, leading to abundant sputtering. The more distant peak at $\xi \cong -x_c$ is due to so-called indirect hits, in which the ion is first reflected from the lower terrace and then hits the step edge. Note that indirect hits are less productive for both surfaces investigated here; but for the unreconstructed surface its reduction is more pronounced. The reduction of the indirect-hit peak is characteristic of strongly corrugated surfaces,⁹ since these deflect the projectile sideways such that they may miss the step edge. Also, due to the geometry of the unreconstructed surface, the step-edge atoms are shadowed by the walls of the V-shaped troughs from the approaching ion. The minimum between the two peaks has been termed the channeling dip, since ions impinging at around $\xi \cong -x_c/2$ do not hit the step edge but are subsurface channeled below the upper terrace and create little damage or sputtering. Also, the unreconstructed surface shows a minimum between the direct- and indirect-hit peaks. It is due to the shadowing mechanism mentioned above: the walls of the V-shaped troughs shadow the step-edge atom from the approaching ion.

VII. CONCLUSIONS

From our atomistic simulations of the impact of 3 keV Ar ions at grazing incidence onto a stepped Si (100) surface, we can draw the following conclusions:

(1) $\langle 110 \rangle$ channels possess the largest critical angle in Si, around 10° for our case. However, they are not accessible for subsurface channeling in an unreconstructed crystal, since the large surface energy barrier prevents ions from entering these channels.

(2) However, surface reconstruction of Si (100) creates new channels immediately under the surface dimers. If the ion-incidence geometry is favorable—incidence azimuth aligned along $\langle 110 \rangle$, the ion approaching an unbonded B step—the ion can enter these channels. A subsurface-channeled ion can also penetrate deeper into the crystal and channel in bulk $\langle 110 \rangle$

channels by the mechanism of channel switching. Without surface reconstruction no subsurface channeling can occur.

(3) An ion which hits the surface within the critical distance x_c [Eq. (2)] of the step has a high probability of becoming subsurface channeled. However, the channeling lengths are quite short, of the order of 1 oscillation, 35 Å. We also find a small percentage of long-channeled particles with channeling lengths of more than 200 Å.

(4) Long-channeled ions create characteristic damage patterns in the form of a long-ranged destruction of the dimer row under which it channels. Ions which experience violent dechanneling create extended surface-vacancy islands, which can be found behind the surface step and detached from it. A third class of damage is provided by direct hits onto the step edge, which damage it locally and are responsible—under prolonged bombardment—for step retraction.

(5) Sputtering shows a characteristic dependence on the distance of the ion-impact point from the step edge. The highest sputter yields are obtained if the ion directly hits the step edge; a second, but minor, maximum is found for indirect hits, where the ion hits the step edge only after reflection from the lower terrace. Since ions impinging on the surface between these two positions have a high probability of becoming channeled under the upper terrace, the sputter yield for these events is almost zero.

(6) From a comparison of previous work^{5–8} on subsurface channeling in Pt with our present results on Si, we can draw the following conclusions: The phenomenon of subsurface channeling appears to be quite widespread, as it is found both for fcc metals and for tetragonally bonded semiconductors. Ions can enter the channel via surface steps; however, for the case of Si, surface reconstruction was necessary to make the channel accessible for the projectile. In all cases, channeled ions create characteristic elongated damage patterns, aligned with the incident ion direction; this feature allows for the identification of subsurface-channeled ions in experiment.

ACKNOWLEDGMENTS

This work has been supported by the *Deutsche Forschungsgemeinschaft* via the Research Unit 845 *Self-Organized Nanostructures Induced by Low-Energy Ion Beam Erosion*. Stimulating discussions with Th. Michely are gratefully acknowledged.

*<http://www.physik.uni-kl.de/urbassek/>; urbassek@rhrk.uni-kl.de

¹G. Carter and V. Vishnyakov, *Phys. Rev. B* **54**, 17647 (1996).

²J. Erlebacher, M. J. Aziz, E. Chason, M. B. Sinclair, and J. A. Floro, *Phys. Rev. Lett.* **82**, 2330 (1999).

³R. Gago, L. Vazquez, R. Cuerno, M. Varela, C. Ballesteros, and J. M. Albella, *Nanotechnology* **13**, 304 (2002).

⁴B. Ziberi, M. Cornejo, F. Frost, and B. Rauschenbach, *J. Phys.: Condens. Matter* **21**, 224003 (2009).

⁵A. Redinger, H. Hansen, U. Linke, Y. Rosandi, H. M. Urbassek, and T. Michely, *Phys. Rev. Lett.* **96**, 106103 (2006).

⁶H. Hansen, A. Redinger, S. Messlinger, G. Stoian, Y. Rosandi, H. M. Urbassek, U. Linke, and T. Michely, *Phys. Rev. B* **73**, 235414 (2006).

⁷Y. Rosandi and H. M. Urbassek, *Nucl. Instrum. Meth. B* **256**, 373 (2007).

⁸A. Redinger, Y. Rosandi, H. M. Urbassek, and T. Michely, *Phys. Rev. B* **77**, 195436 (2008).

⁹A. Redinger, S. Standop, T. Michely, Y. Rosandi, and H. M. Urbassek, *Phys. Rev. Lett.* **104**, 075501 (2010).

¹⁰A. Redinger, S. Standop, Y. Rosandi, H. M. Urbassek, and T. Michely, *New J. Phys.* **13**, 013002 (2011).

¹¹R. M. Bradley and J. M. E. Harper, *J. Vac. Sci. Technol. A* **6**, 2390 (1988).

¹²T. Michely and J. Krug, *Islands, Mounds, and Atoms*, Springer Series in Surface Science Vol. 42 (Springer, Berlin, 2004).

- ¹³N. Kalyanasundaram, M. Ghazisaeidi, J. B. Freund, and H. T. Johnson, *Appl. Phys. Lett.* **92**, 131909 (2008).
- ¹⁴S. A. Norris, J. Samela, L. Bukonte, M. Backman, F. Djurabekova, K. Nordlund, C. S. Madi, M. P. Brenner, and M. J. Aziz, *Nat. Commun.* **2**, 276 (2011).
- ¹⁵W. Mönch, *Semiconductor Surfaces and Interfaces*, Springer Series in Surface Sciences Vol. 26, 2nd ed. (Springer, Berlin, 1995).
- ¹⁶D. R. Bowler and M. G. Bowler, *Phys. Rev. B* **57**, 15385 (1998).
- ¹⁷F. H. Stillinger and T. A. Weber, *Phys. Rev. B* **31**, 5262 (1985).
- ¹⁸J. F. Ziegler, J. P. Biersack, and U. Littmark, *The Stopping and Range of Ions in Solids* (Pergamon, New York, 1985).
- ¹⁹D. J. Chadi, *Phys. Rev. Lett.* **43**, 43 (1979).
- ²⁰L. Pauling and Z. S. Herman, *Phys. Rev. B* **28**, 6154 (1983).
- ²¹A. Ramstad, G. Brocks, and P. J. Kelly, *Phys. Rev. B* **51**, 14504 (1995).
- ²²J. R. Beeler Jr., *Radiation Effects Computer Experiments* (North-Holland, Amsterdam, 1983).
- ²³Y. Rosandi, A. Redinger, T. Michely, and H. M. Urbassek, *Nucl. Instrum. Meth. B* **267**, 2769 (2009).
- ²⁴H. M. Urbassek, C. Anders, and Y. Rosandi, *Nucl. Instrum. Meth. B* **269**, 947 (2011).
- ²⁵A. Friedrich and H. M. Urbassek, *Surf. Sci.* **547**, 315 (2003).
- ²⁶J. Lindhard, *Mat. Fys. Medd. K. Dan. Vidensk. Selsk.* **34**, 14 (1965).
- ²⁷S. Zimmermann and H. M. Urbassek, *Nucl. Instrum. Meth. B* **255**, 208 (2007).
- ²⁸P. V. Zalm, *J. Appl. Phys.* **54**, 2660 (1983).
- ²⁹K. Wittmaack, *Phys. Rev. B* **68**, 235211 (2003).
- ³⁰W. Eckstein, in *Sputtering by Particle Bombardment*, Topics in Applied Physics Vol. 110, edited by R. Behrisch and W. Eckstein (Springer, Berlin, 2007), p. 33.